Aerospace Science and Technology 129 (2022) 107822

Contents lists available at ScienceDirect

Aerospace Science and Technology

www.elsevier.com/locate/aescte

A novel ablative material for thermal protection system: Carbon fiber/polysiloxane composites

Yanan Hou [a,1], Colin Yee [a,1], Wei Li [a,2], Joseph H. Koo [a,*,3], Liguo Li [b,4], Ben Rech [c,5], William Fahy [c,5], Hao Wu [c,5], Jarrod J. Buffy [d,6]

[a] The University of Texas at Austin, Austin, TX 78712, USA
[b] Advanced Composites International, Round Rock, TX 78665, USA
[c] KAI, LLC, Austin, TX 78739, USA
[d] Techneglas LLC, Perrysburg, OH 43551, USA

ARTICLE INFO

Article history:
Received 19 April 2022
Received in revised form 17 June 2022
Accepted 15 August 2022
Available online 19 August 2022
Communicated by Marwan Al-Haik

ABSTRACT

Fiber reinforced composite materials are widely used in the aerospace industry due to their high strength to weight ratio. One of their applications is as an ablative material placed at the outermost layer of a thermal protection systems (TPS). A TPS requires the ablative material to have low density, low thermal conductivity, high temperature resistance, formation of a stable and high shear strength char. This paper introduces a carbon fiber (CF) reinforced polysiloxane (UHTR) composite material processed and fabricated in a laboratory environment. The fabrication method of this material is illustrated in detail. Thermal, ablation, flammability, and mechanical properties of the CF/UHTR material are characterized and compared to a commercial model ablative material, MX4926. MX4926 is a carbon fiber phenolic (CF/Ph) composite material manufactured by Solvay-Cytec. In this study, the carbon fiber used to make the CF/UHTR material is a PAN-based 8-harness fabric provided by Hexcel. The polymer matrix, UHTR, is a colorless semi-solid polysiloxane resin manufactured by Techneglas LLC. Raw materials are firstly made into CF/UHTR prepreg sheets through a hot-melt process and then compression molded into molding compound (MC) samples or two-dimensional (2D) laminates by a hot press. All samples for testing are post cured in a programmable oven at 350 °C for 2 hours. The density of the fully-cured material is measured by the water displacement method. Thermal stability, flammability, and ablation properties of the material (in the format of MC) are characterized using thermogravimetric analysis (TGA), microscale combustion calorimeter (MCC), and oxyacetylene test bed (OTB) with three different heat fluxes. Mechanical properties of the material (in 2D laminates) are measured by a universal testing machine (UTM) to the ASTM standards. Testing results of the CF/UHTR material are compared with the commercial model ablative material, MX4926. Microstructures of the CF/UHTR material before and after mechanical and ablation tests are investigated and compared by an optical microscope and scanning electron microscopy (SEM) to further study the failure mode of the material.

1. Introduction

Thermal protection system (TPS) is an important component in the aerospace industry. On many occasions, high temperature ablative material is placed at the most outer layer of a TPS [1] to protect the components or structures of the functional parts, such as space vehicles during the reentry stage [2] or rocket motor nozzles [3]. Most ablative materials are reinforced organic resin composites [4] due to their low densities, good ablation, and insulative properties. For example, the Apollo command modules (CM) used a low-density material, Avcoat 5026-39/HC-G, as their heat shield started in late 1960s. Avcoat 5026-39/HC-G is an epoxy-novolac resin filled fiberglass honey comb material [5], with a

* Corresponding author.
E-mail address: jkoo@mail.utexas.edu (J.H. Koo).
[1] Texas Materials Institute, The University of Texas at Austin.
[2] Walker Department of Mechanical Engineering, The University of Texas at Austin.
[3] KAI, LLC, and Polymer Nanocomposites Technology Lab, Walker Department of Mechanical Engineering, The University of Texas at Austin.
[4] Advanced Composites International, LLC.
[5] KAI, LLC.
[6] Techneglas LLC.

https://doi.org/10.1016/j.ast.2022.107822
1270-9638/

Nomenclature

CF	Carbon Fiber	MCC	Microscale Combustion Calorimeter
CFF	Carbon Fiber Fabric	OTB	Oxy-acetylene Test Bed
CM	Command Module	POSS®	polyhedral oligomeric silsesquioxane
CF/Ph	Carbon Fiber Phenolic	SEM	Scanning Electron Microscopy
DoD	Department of Defense	TGA	Thermogravimetric Analysis
HRC	Heat Release Capacity	TPS	Thermal Protection Systems
HRR	Heat Release Rate	UHTR	Ultra-High Temperature Resin
MC	Molding Compound	UTM	Universal Testing Machine

density of 0.51 g/cc, a char density of about half of its virgin material density, an ablating temperature (start of pyrolysis) of 316 °C, and a recession temperature (start of recession) of about 970 °C [6]. The Apollo CM TPS were designed to tolerate a peak temperature of up to 5000 °F (2760 °C) [1] and experienced a peak heat flux of about 500 W/cm^2 [4] with reentry times range between 800 to 900 s for operational lunar missions [1]. Avcoat 5026-39/HC-G has the advantage of low density and has presented good ablation and insulative properties for medium heat fluxes, however, its manufacturing process is very time consuming and labor intensive because all the fiberglass honeycombs are required to be injected and inspected by meticulous workers. For the Mars-pathfinder project with mild heat flux (~25 W/cm^2) environment in 1970s, SLA-561V was used as the heat shield material [4]. SLA-561V is a cork-filled and glass fiber-reinforced room-temperature curing elastomeric silicone in a phenolic honeycomb [7]. The material was designed to tolerate a peak shear stress of 158 N/m^2 and the heat flux at peak shear location is about 75 W/cm^2. SLA-561V has presented good resistance to shear force without excessive char removal or spallation [7] in mild heat flux conditions. For the high heat flux environments, such as Pioneer Venus in late 1970s and Galileo (Jupiter) in late 1980s, a carbon phenolic material was used for the TPS, where peak heat flux reached about 10,000 W/cm^2 [8].

Based on the Galileo mission, fully dense carbon phenolic is the only material that may be inherited for high heat flux environments. But the recession data from the Galileo mission also showed that the weight fraction of its TPS could not be reduced or should even be increased for a similar Jovian equatorial entry probe mission to be safer. The weight fraction of the TPS of the Galileo was already 50% [8]. However, there are limited research on ablative TPS materials, especially for high heat flux environments, in the past 30 years, partially due to NASA's "risk averse" philosophy relative to TPS [8]. For example, Koo et al. conducted two comprehensive reviews on the effects of nanocomposites on the performance of TPS and their ablation mechanisms, including carbon nanofibers, polyhedral oligomeric silsesquioxane (POSS®), nanosilicas, and so on [9–11]. Kim et al. developed a 3D printable polyetherimide nanocomposite for TPS and found its good potential for TPS application, but only for low heat flux environments [12]. There are also some researchers focused on reusable TPS, using metallic materials as solutions for the high heat flux environments and achieved success to a certain extent, but limited to the higher density of metallic alloys [13,14].

This paper introduces a carbon fiber (CF) reinforced polysiloxane composite. The material is fabricated into prepreg, laminate and molding compound for testing. Its potential for TPS applications is evaluated by comparing it with a commercial model ablative material, MX4926 [15–17]. MX4926 is a C/Ph ablative material manufactured by Solvay-Cytec and is considered as a legacy ablative used by US Department of Defense (DoD) as well as NASA for solid rocket motor and TPS applications. In this study, thermogravimetric analysis (TGA) is used to evaluate the thermal stability and char yield of the material, microscale combustion calorimeter (MCC) is used to study the flammability of the material, and oxyacetylene test bed (OTB) is used for aerothermal ablation testing to simulate the reentry conditions to investigate the performance of the material at exposure to medium to high heat fluxes. In addition, optical microscope and scanning electron microscopy (SEM) are used to investigate the microstructures of the material before and after the OTB tests to understand the ablation mechanisms of the material. Universal testing machine (UTM) is used to measure the mechanical properties of the material.

2. Experimentation

2.1. Materials

The reinforcement of the composites introduced in this research is a carbon fiber fabric provided by Hexcel. The fabric is made of PAN-based carbon fibers, AS4. The matrix is a polysiloxane resin provided by Techneglas LLC. Basic properties of the carbon fabric, the PAN-based carbon fiber, and the polysiloxane resin are summarized in Tables 1–3.

Table 4 lists material compositions of the lab-made CF/UHTR material in comparison to that of MX4926, a fully dense commercial carbon phenolic ablative material. The density of the CF/UHTR is about 3% lower comparing to MX4926.

2.2. Fabrication of samples

The reinforcement fabrics and semi-solid polymer matrix are firstly combined into CF/UHTR prepreg sheets using a hot-melt procedure. CF/UHTR prepreg sheets are then cut into 0.5 inch by 0.5 inch squares to make CF/UHTR MC samples or compressed directly to make CF/UHTR 2D laminates.

2.2.1. Ideal matrix weight ratio calculation

The volume ratio of voids in the carbon fiber fabrics can be calculated by Eq. (1),

$$V_{void}\% = \frac{\rho_{CF} - \rho_{CFF}}{\rho_{CF}} * 100\%, \tag{1}$$

where ρ_{CF} is the density of the carbon fiber, and ρ_{CFF} is the density of the carbon fiber fabrics, which can be calculated by dividing the area weight of the fabric by its thickness.

The ideal matrix weight ratio is defined as the weight ratio of the matrix when the volume ratio of the matrix equals to the volume ratio of the voids in the fabric, and can be calculated by Eq. (2),

$$W_{matrix}\% = \frac{\rho_{matrix} * V_{void}\%}{\rho_{matrix} * V_{void}\% + \rho_{CF} * (1 - V_{void}\%)} * 100\%, \tag{2}$$

Table 1
Summary of basic properties of the reinforcement in CF/UHTR.

Reinforcement	Style	Weave	Count Warp	Count Fill	Warp Yarn	Fill Yarn	Area Weight, g/m^2	Thickness, mm
Carbon fiber fabrics	AGP370-8H	8-harness	22	23	AS4GP 3K	AS4GP 3K	373	0.42

Table 2
Summary of basic properties of the carbon fiber in CF/UHTR.

Carbon Fiber	Tensile Strength, ksi	Tensile Modulus, msi	Strain (%)	Density, g/cc
AS4	638-650	33.5	1.8	1.79

Table 3
Summary of basic properties of the matrix in CF/UHTR.

Matrix	Appearance	Viscosity, cPs	T_g, °C	Density, g/cc
UHTR 6398-S	Colorless and semi-solid	20k @ 70 °C	>500	1.2

Table 4
Material compositions.

Material ID	Density, g/cc	Reinforcement, wt.%	Matrix, wt.%	Filler, wt.%	Volatile Content, wt.%
MX4926	1.47	Rayon-based carbon fiber, 41–56	SC-1008 phenolic, 31–37	Carbon black, 11–16	2–6
CF/UHTR	1.43	PAN-based carbon fiber, 57–60	UHTR 6398-S polysiloxane, 40–43	None	None

Fig. 1. Pre-cut carbon fiber mat (12 inches by 12 inches) laid on a hot press pre-heated at 150 °C).

where ρ_{matrix} is the density of the matrix. Inserting values listed in Tables 1–2, the ideal matrix weight ratio in this study is 40.5%.

2.2.2. Hot-melt prepreg fabrication

A hot press and a programmable oven are used in the hot-melt process. Carbon fiber fabrics are cut into 12 inches by 12 inches mats for easy handling, as shown in Fig. 1. The weight of each mat is measured and recorded as W_{CF}. The weight of UHTR is calculated based on the ideal matrix weight ratio. Extra 10 wt.% UHTR is added to compensate the waste loss during the process. UHTR is pre-heated at 100 °C for 30 min to lower its viscosity.

To make CF/UHTR prepreg sheets, a carbon fiber mat is laid on the bottom plate of a hot press that is preheated at 150 °C, as shown in Fig. 1. Pre-heated UHTR is spread evenly on the carbon fiber mat using a heat-resistant silicone scraper. The setup is then pressed under 5,000 psi at 150 °C for 5 min, before being taken out of the hot press and cooling to room temperature on a flat surface. Top and bottom peel plies are applied for easy cleaning. The prepreg is weighted after the top and bottom peel plies peeled and excess UHTR trimmed. The weight is recorded as $W_{pre\text{-}preg}$. The real matrix weight ratio is calculated by Eq. (3).

$$W_{matrix}\% = \frac{W_{pre\text{-}preg} - W_{CF}}{W_{pre\text{-}preg}} * 100\%, \tag{3}$$

In this study, the matrix weight ratios range from 40.2% to 43.2%.

2.2.3. Molding compound (MC) process

A hot press and a cylindrical mold are used in this process. Pre-made carbon fiber/UHTR prepregs are cut into 0.5 inch by 0.5 inch squares using a paper cutter, as shown in Fig. 2. Pre-weighted CF/UHTR prepreg squares are placed in a 3-inch diameter three-part cylindrical mold and compressed under 2,500 psi at 150 °C for 24 hours using a hot press. The temperature of the hot press is then increased to 340 °C (the maximum temperature of the hot press) and soaked for 2 hours to further cure the material before demolding. To make CF/UHTR MC sample of 3 inches in diameter and 0.5 inch in thickness, as shown in Fig. 3, 85 g prepreg squares are approximately needed. The CF/UHTR MC samples are post cured at 350 °C for 2 hours in a programmable oven before testing.

2.2.4. Two-dimensional (2D) lamination process

A hot press is used in this process. Six layers of pre-made CF/UHTR prepregs are cut into 11 inches by 11 inches sheets, stacked up symmetrically (3 layers facing up, 3 layers facing down), and compressed under 2,500 psi at 150 °C for 24 hours by a pre-heated hot press. The temperature of the hot press is then increased to 340 °C for 2 hours to further cure the laminate. Top and bottom peel plies are used for easy cleaning. The laminate is post cured at 350 °C for 2 hours before cutting into mechanical testing samples to ASTM standards. Fig. 4 shows a CF/UHTR 2D laminate sample.

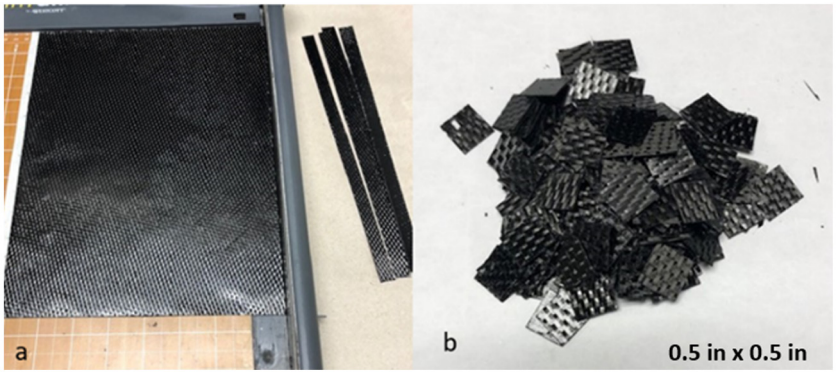

Fig. 2. CF/UHTR prepregs are into (a) 0.5-inch width strips; (b) 0.5 inch by 0.5 inch squares.

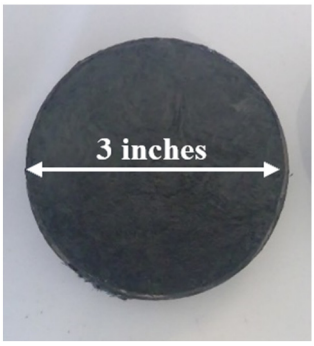

Fig. 3. A CF/UHTR MC sample (3 inches in diameter and 0.5 inch in thickness).

Fig. 4. A CF/UHTR 2D laminate sample (11 inches by 11 inches by 0.1 inches).

2.3. Material characterization

2.3.1. Thermogravimetric Analysis (TGA)

A thermogravimetric Analyzer (TGA/DSC 1 STAR® System by Mettler Toledo) is used to compare the thermal stability and char yields of the MX4926 and CF/UHTR composites. TGA measures weight losses of testing materials as temperature increasing. In TGA tests, both materials (∼15 mg) are dried at 150 °C isothermally for 30 minutes and directly heated up to 1,000 °C at 20 °C/min in both air and nitrogen environments. Char yield of the material is defined as the residue weight of the material at 1,000 °C divided by its weight after the isothermal dying period evaluated in nitrogen with a heating rate of 20 °C/min.

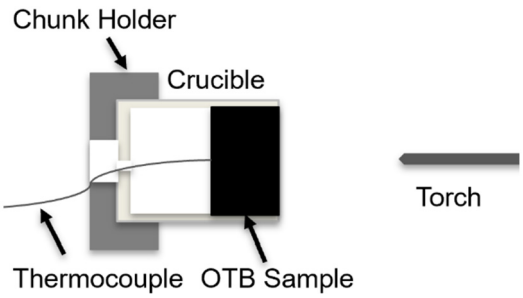

Fig. 5. Sketch of the OTB setup.

2.3.2. Microscale Combustion Calorimetry (MCC)

A Microscale Combustion Calorimeter (MCC2, Govmark, Inc.) is used to study thermal combustion properties of the materials according to ASTM D7309-2007. MCC measures heat release rates of a material as temperature increases. In MCC tests, both materials (2–3 mg) are heated up rapidly from 100 °C to 700 °C at 1 °C/s in the environment of 80 mL/min nitrogen and 20 mL/min oxygen. Heat release rate and heating rates are recorded as temperatures. From MCC results, the heat release capacity (HRC), peak heat release rate (HRR), and the temperature of peak HRR of the material can be obtained. At least three repeated samples of each material are evaluated to calculate error bars according to the ASTM standard.

2.3.3. Oxyacetylene Test Bed (OTB)

The OTB aerothermal ablation test is used to study the ablation properties of the materials. CF/UHTR MC and MX4926N MC (material ID of MX4926 in the format of molding compound) samples are cut into cylindrical OTB test models of 30 mm (1.18 inches) in diameter and 12.7 mm (0.5 inch) in thickness by a waterjet cutter. The OTB test model is mounted in a crucible with an ID that is slightly larger than the diameter of the OTB test model with a silicone rubber. The top surface of the OTB sample is leveled with the top of the crucible. The depth of the crucible is larger than the thickness of the OTB sample. A sheathed K-type thermocouple is inserted through a 2 mm diameter hole at the bottom of the crucible and contacted the backside of the OTB test model. During the OTB aerothermal test, the crucible is clamped on a chunk holder. A torch with a #4 victor welding tip approaches the top surface of the OTB test model to simulate reentry conditions. A ratio of 4:3 oxygen: acetylene is used as throughout OTB aerothermal testing. Fig. 5 shows a sketch of the OTB setup.

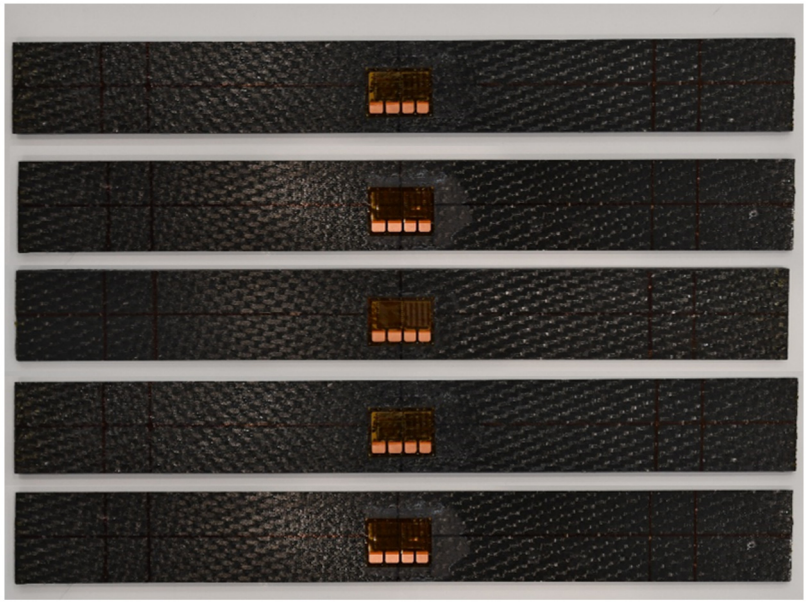

Fig. 6. Tensile testing samples with strain gauge.

Table 5
Simulated reentry conditions.

Condition		Ablation Parameter, kJ/cm^2 (i.e., heat flux X exposure time)
Heat Flux, W/cm^2	Exposure Time, s	
500	60	30
1,000	60	60
1,500	60	90

Three conditions are simulated, as listed in Table 5. Various heat fluxes are obtained by adjusting the standoff distance between the torch and the top surface of the OTB sample and calibrated by a Vatell Gardon heat flux transducer (Thermogage 1000-54).

Heights (or thicknesses) and masses of OTB test models are measured before and after OTB aerothermal tests. After-testing heights are taken at the lowest point of the samples. Backside temperatures during the OTB tests are measured by the thermocouple shown in Fig. 5. Top surface temperatures are measured by a 2-color IR pyrometer. OTB results are presented as recession percentages (Eq. (4)), mass losses (Eq. (5)), surface and backside temperatures versus ablation parameters.

$$Recession\ Percentage = \frac{Initial\ Height\text{-}Final\ Height}{Initial\ Height} * 100\%, \quad (4)$$

$$Mass\ Loss = \frac{Initial\ Weight\text{-}Final\ Weight}{Initial\ Weight} * 100\%, \quad (5)$$

2.3.4. Mechanical test

A Shimazu universal testing machine is used to evaluate the mechanical properties of the material. Tensile properties of CF/UHTR 2D laminate samples are tested to ASTM D3039. Five samples are used for the test. Strain gauges (CEA-09-250UT-350) by Micro-Measurements are attached in the middle of each tensile bar to measure the strain during the tests, as shown in Fig. 6. Flexural properties of CF/UHTR 2D laminate samples are tested to ASTM D790, strain gauges (EA-06-125BZ-350/LE) by Micro-measurements are applied. Compressive properties of CF/UHTR 2D laminate samples are tested to ASTM D6641, with strain gauges SGD-5/350-LY41 by Omega engineering, Inc.

2.3.5. Microstructures

A Keyence optical microscopy and a SEM (FEI Quanta 650 ESEM) are used to investigate microstructure changes of the material before and after mechanical and OTB aerothermal tests. SEM samples are coated with gold by an EMS putter coater. A voltage of 20 kV is used for the tests. Observation results help further understanding of the failure mode of the material and provide guidance for material improvements.

3. Results and discussion

3.1. TGA thermal stability test results

Fig. 7 shows weight changes of CF/UHTR MC and MX4926N MC samples at elevated temperatures in nitrogen and air. In both tests in air and nitrogen, MX4926N MC samples (green dash dotted line and blue dash line) have lost about 2% weights during the isothermal drying periods (150 °C for 30 min). This is due to the phenolic matrix in MX4926N MC, which is known for moisture taken. The TGA results show that MX4926N MC (green dash dotted line) decomposes after 200 °C, followed by a quick decomposition at around 400 °C and a quicker decomposition at around 520 °C. CF/UHTR MC (red solid line) is stable up to 400 °C followed by one quick single step decomposition process. Char yield is defined as the weight of the material at 1,000 °C divided by its weight after the isothermal period in nitrogen environment. The heating rate is set at 20 °C/min. As listed in Table 6, the char yield of MX4926N MC is calculated to be 84%, which is remarkably high. The char yield of CF/UHTR MC at the same condition is even higher, yields 93%. In air, both materials show similar tends to their performances in nitrogen at temperatures below 600 °C. At elevated temperatures, both materials are further decomposed due to oxidative reactions in the presence of oxygen. CF/UHTR MC (orange dotted line) has a residue weight of 25% at 920 °C and stabilized to the end of the test, whereas MX4926N MC (blue dash line) is completely decomposed at 880 °C. These TGA results already showed that the thermal stability of CF/UHTR MC is significantly better than the model ablative MX4926N MC, a first indication that the CF/UHTR material may be a better ablator than the MX4926N MC material.

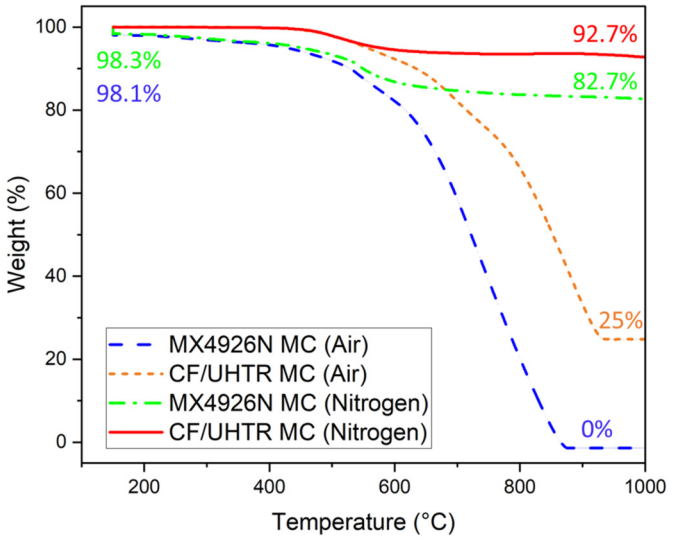

Fig. 7. TGA mass loss curves (TGA, heating rate of 20 °C/min in air and N_2). (For interpretation of the colors in the figure(s), the reader is referred to the web version of this article.)

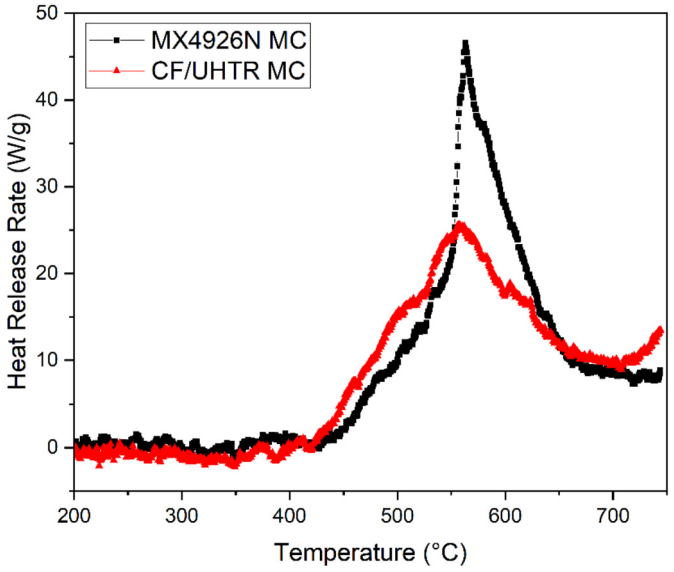

Fig. 8. Representative HRR curves (MCC, heating rate of 1 °C/s in 20% O_2 and 80% N_2).

Table 6
Char Yield Comparison of CF/UHTR MC and MX4926N MC.

Material ID	CF/UHTR MC	MX4926N MC
Char Yield, %	92.7	84.1

3.2. MCC flammability test results

Fig. 8 shows representative heat release rate curves of the CF/UHTR MC and MX4926N MC materials over temperatures. MX4926 is known for its good flammability properties. The peak HRR of MX4926N MC is 46.6 W/g, while that of the CF/UHTR MC is 25.6 W/g, which is even 45% lower comparing to MX4926N MC. Three samples of each material are evaluated, all results are summarized in Fig. 9. CF/UHTR MC presents a significantly smaller peak HRR and HRC. In addition, the temperature of the peak HRR of CF/UHTR MC is lower than that of the MX4926N MC material.

3.3. OTB ablation test results

Fig. 10 (a) shows recession percentages of the CF/UHTR MC and MX4926N MC materials over ablation parameters. The shades areas represent the error range. Ablation parameter is defined as the heat flux multiplies the time that the material exposed to the OTB flame, this represents the heat load imposing on the material. Both materials present negative recession percentages at all tested conditions, which implies the materials have swelled more than receded during the OTB aerothermal tests. To separate the swell and material loss, the mass losses of both materials are plotted as ablation parameters, as shown in Fig. 10 (b).

Fig. 10 (b) shows that the mass losses of both materials increase as the ablation parameter increases. The shaded areas represent the error range. Mass losses of the CF/UHTR MC are approximately 1/8 of those of the MX4926N MC material in all test conditions, which indicates that the CF/UHTR MC has better ablation resistant property than the MX4926N MC.

Fig. 11 shows the top surface temperatures and the backside heat-soaked temperatures of CF/UHTR MC and MX4926N MC in the OTB ablation tests. The shaded areas represent the error range. Temperatures of both materials are similar in all testing conditions. Surface temperatures of both materials have reached above 1,800 °C, the backside heat-soaked temperatures of both materials are remained below 250 °C. These results indicate that both materials have incredibly good thermal insulation property.

3.4. Mechanical test results

Fig. 12 (a) shows a representative stress and strain curve of an CF/UHTR 2D laminate sample in a tensile test. The fracture is marked by "x." The maximum stress is defined as the ultimate tensile stress. The slop of the linear zone defines the Young's Modulus. Five tests are conducted to calculate the error bars, results are summarized in Fig. 12 (b). Tensile tests results show that CF/UHTR laminates have an averaged tensile strength of 49.6 ksi, which is 2.4 times higher than the tensile strength of MX4926 laminates. The averaged Young's Modulus of CF/UHTR laminates is 6.6 msi. This is 2.64 times higher than the MX4926 laminates. Elongation at break values of both materials tend to be low, which is 0.97% for CF/UHTR laminates or 1.2% for MX4926 laminates.

Fig. 13 (a) shows a representative stress-strain curve of a CF/UHTR laminate sample in a three-point bending test. The maximum stress is defined as flexural strength. Unlike most metallic material, the fiber reinforced composite laminate material is still able to hold some stress after the fracture. Fig. 13 (b) summaries the flexural properties of the CF/UHTR laminates comparing to those of MX4926 Laminates (provided by MX4926 technical data sheet). CF/UHTR laminates have a slightly higher averaged flexural strength. The flexural modulus of MX4926 is not provided in the technical data sheet. CF/UHTR laminates have an averaged flexural modulus of 8.6 msi.

Fig. 14 (a) shows a representative stress-strain curve of a CF/UHTR laminate sample in a compressive test. The maximum stress is defined as compressive strength of the material. The slop of the curve represents the compressive modulus of the material. Fig. 14 (b) summarizes the compressive properties of CF/UHTR laminates comparing to those of MX4926 laminates. The compressive strength of CF/UHTR laminates is significantly lower than that of MX4926 laminates due to the low compressive strength of UHTR resin comparing to phenolic resin. Microscopy analyses are used to further study the failure modes of the material after mechanical tests.

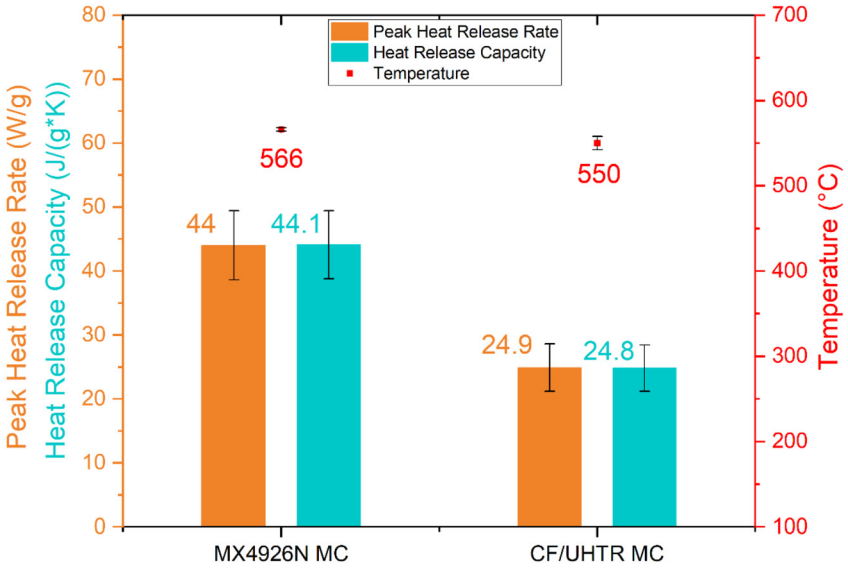

Fig. 9. Summary of MCC results of CF/UHTR MC and MX4926N MC materials.

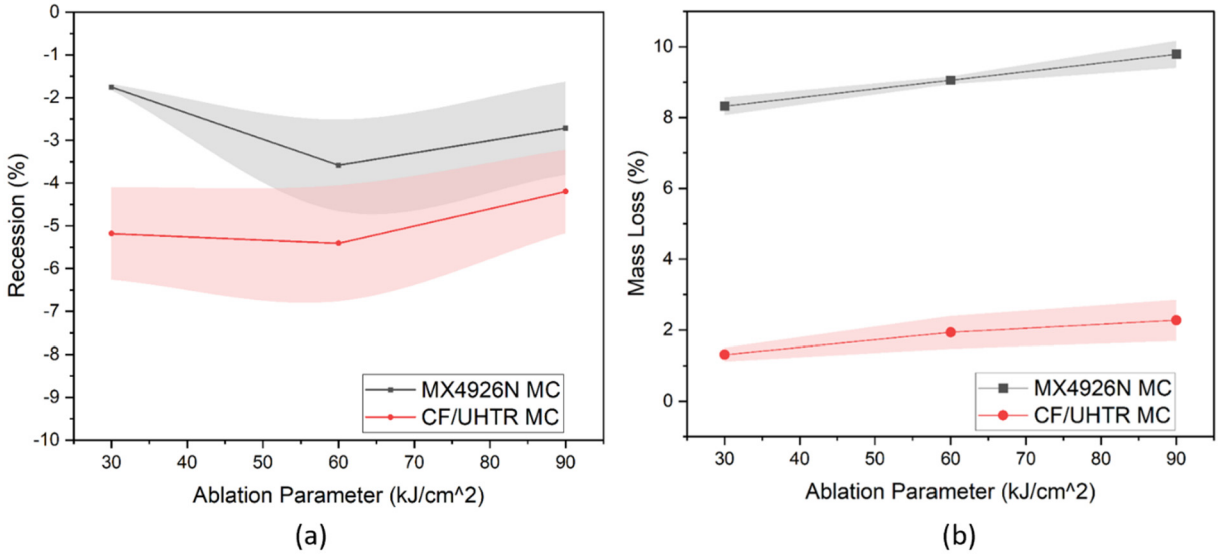

Fig. 10. Summary of recession percentage results in OTB ablation tests: (a) Recession versus ablation parameter; (b) Mass loss versus ablation parameter.

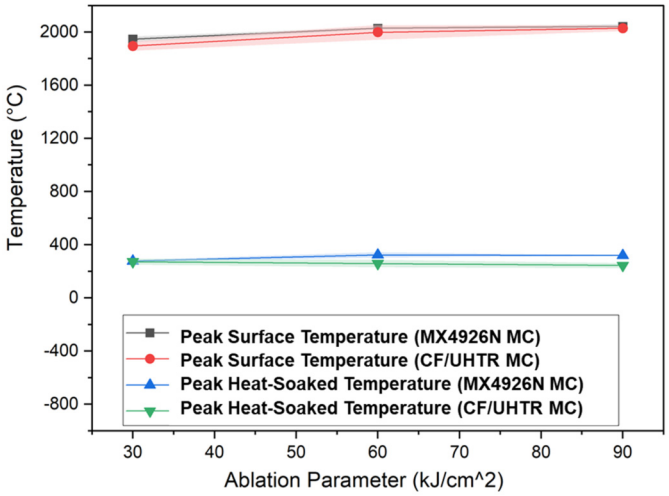

Fig. 11. Summary of temperature results in OTB ablation tests.

3.5. Microstructure analysis

CF/UHTR MC OTB test models before and after OTB ablation tests are embedded in a low temperature curing clear epoxy and cut by a tile saw to investigate their cross-sections (through thickness direction), as shown in Fig. 15. The clear epoxy helps to keep the integrity of the charred OTB samples, especially the ones after OTB ablation tests with high ablation parameters.

Fig. 16 compares the middle area of cross-sections (marked by the yellow square in Fig. 15) of CF/UHTR MC OTB samples before and after OTB ablation tests. Cross sections of the samples after OTB tests do not show obvious char, pyrolysis and virgin zones like traditional ablative materials [4], but show increased amount of voids through the thickness direction comparing to the sample before OTB test. This caused by the strength decreasing of the matrix at elevated temperatures, leading to relaxation of the compressed carbon fibers.

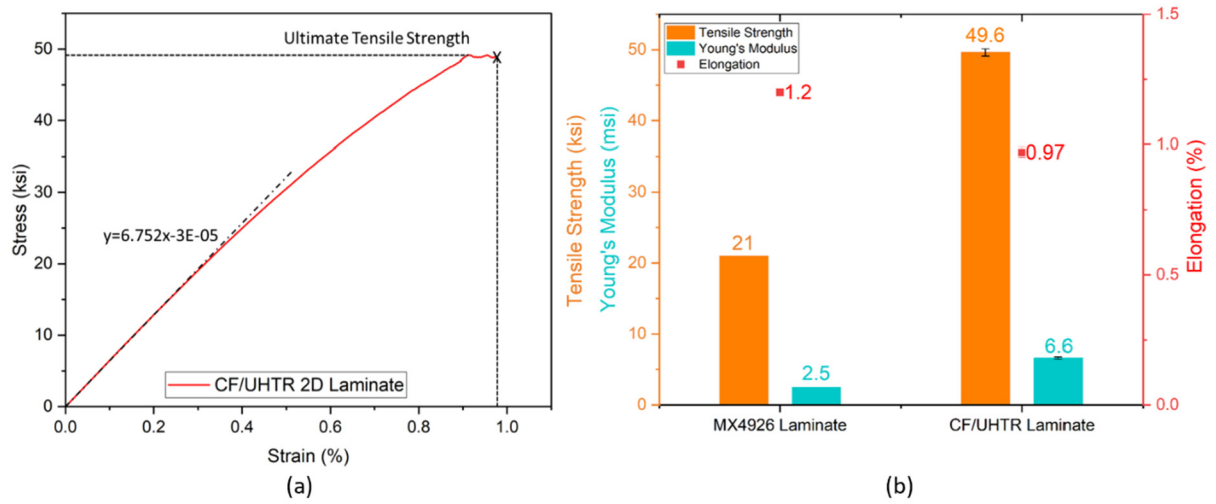

Fig. 12. Summary of tensile properties: (a) Representative stress-strain curve of a CF/UHTR laminate sample in a tensile test; (b) Comparison of tensile properties (MX4926 vs. CF/UHTR).

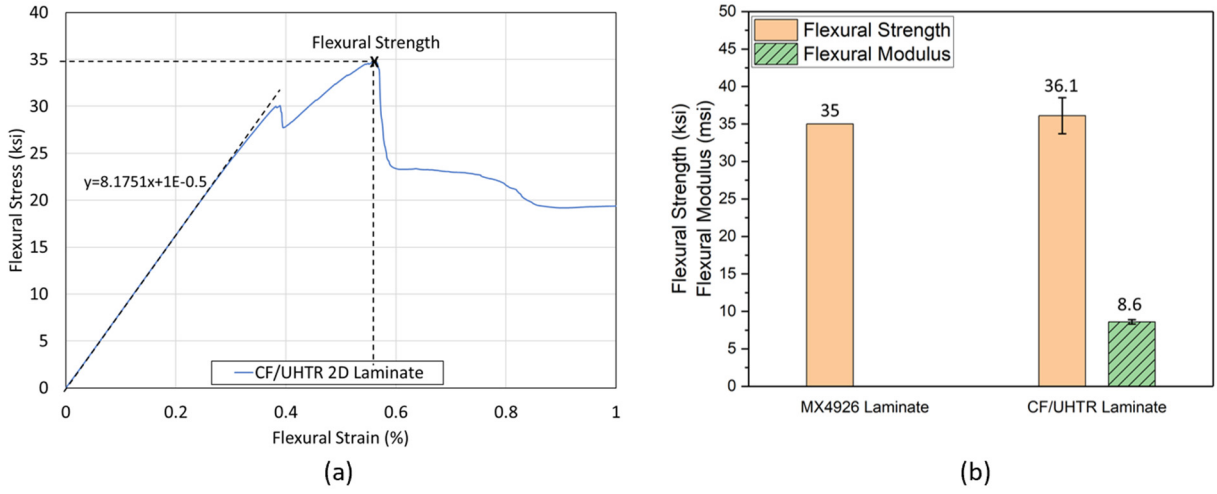

Fig. 13. Summary of flexural properties: a) Representative stress-strain curve of a CF/UHTR laminate sample in a three-points bending test; b) Comparison of flexural properties (MX4926 vs CF/UHTR).

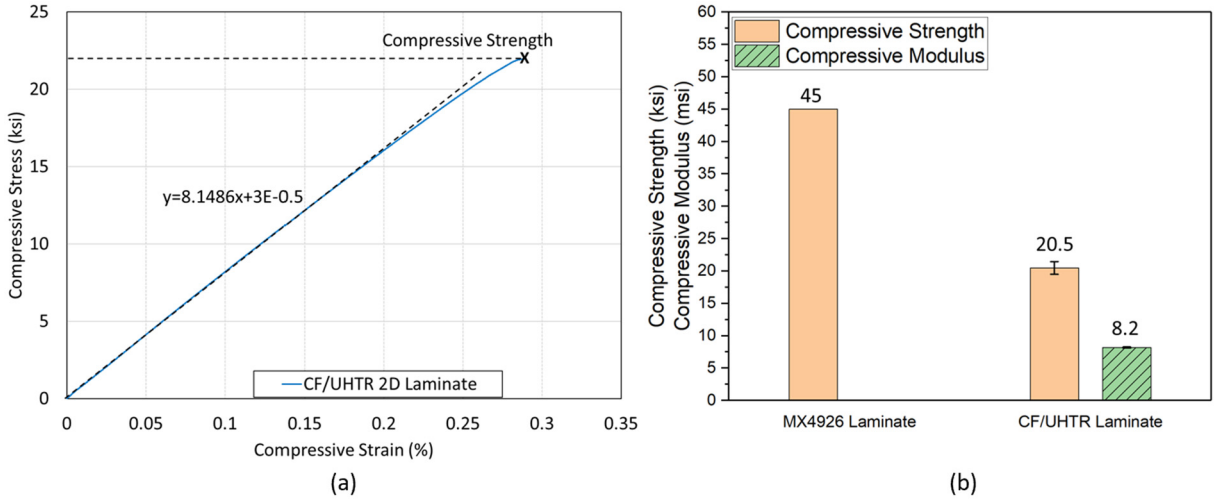

Fig. 14. Summary of compressive properties: a) Representative stress-strain curve of a CF/UHTR laminate sample in a compressive test; b) Comparison of compressive properties (MX4926 vs CF/UHTR).

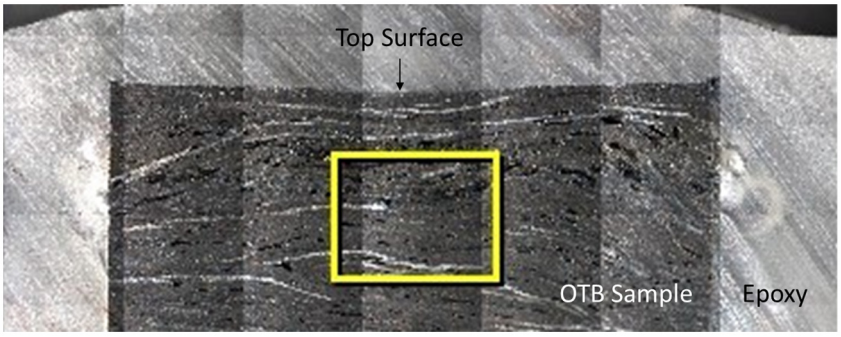

Fig. 15. Representative encapsulated OTB sample for microscopy test.

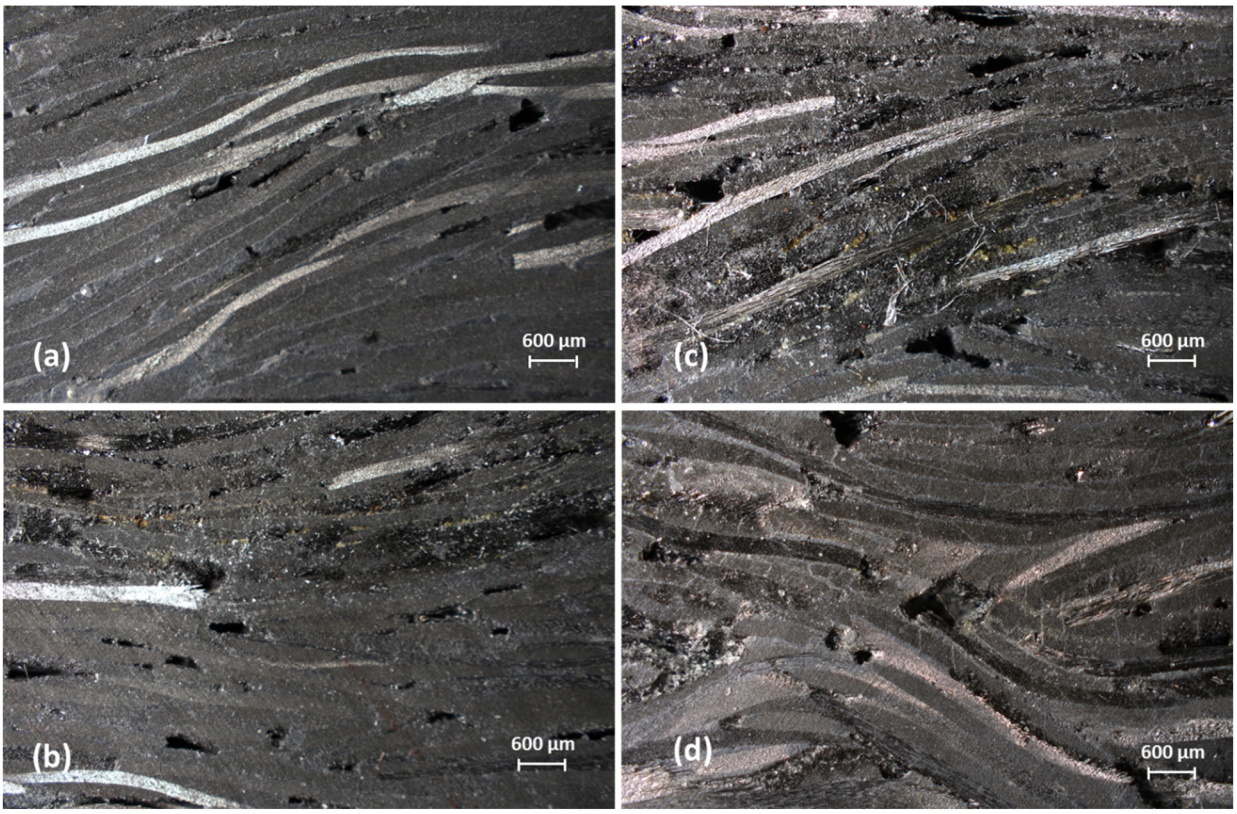

Fig. 16. Cross-section of CF/UHTR OTB samples: (a) before OTB test; (b) AP=30 (kJ/cm^2); (c) AP=60 (kJ/cm^2); and (d) AP=90 (kJ/cm^2).

Fig. 17 compares SEM images of CF/UHTR MC before and after the OTB ablation test with the ablation parameter of 90 kJ/cm^2. As expected, it further shows that after the OTB ablation test, the binding matrix, UHTR, has de-bonded compressed carbon fibers and the fiber relaxation results in material swelling and increasing permeability. The material is expected to eventually recede at higher heat flux or longer exposure time (*i.e.*, at high AP values).

Samples after mechanical tests are studied to understand the failure modes of the material, as shown in Fig. 18. In the tensile test, the material delaminated significantly. In the flexural test, delamination is initiated at the top layers due to compression and bottom layers due to tension. In the compressive test, delamination is initiated in the middle of the material. These results indicate that the bonding between the carbon fiber and the UHTR resin is weak and can be improved by developing a carbon fiber sizing that will be compatible with the UHTR resin.

3.6. Conclusions and future work

In this study, a CF/UHTR composite is introduced and its potential for TPS applications is evaluated. Comparing to the commercial model ablative material, MX4926 (CF/Ph), CF/UHTR material presents lower density, higher moisture resistance, superior thermal stability, significantly better ablation and flammability properties. In mechanical properties testing, CF/UHTR material shows significantly higher tensile strength and comparable flexural properties comparing to MX4926. The compressive strength of the CF/UHTR is dramatically lower than that of the MX4926 due to the lower elongation and compressive strength of UHTR resin comparing to phenolic resin. To enhance the bonding between the carbon fiber with the UHTR resin, compatible carbon fiber sizing with the UHTR resin should be explored. Thermal, flammability, and ablation properties of the CF/UHTR material can be further enhanced by considering CF/ceramic-UHTR polymer nanocomposites in our future studies. Microstructures characterization of the car-

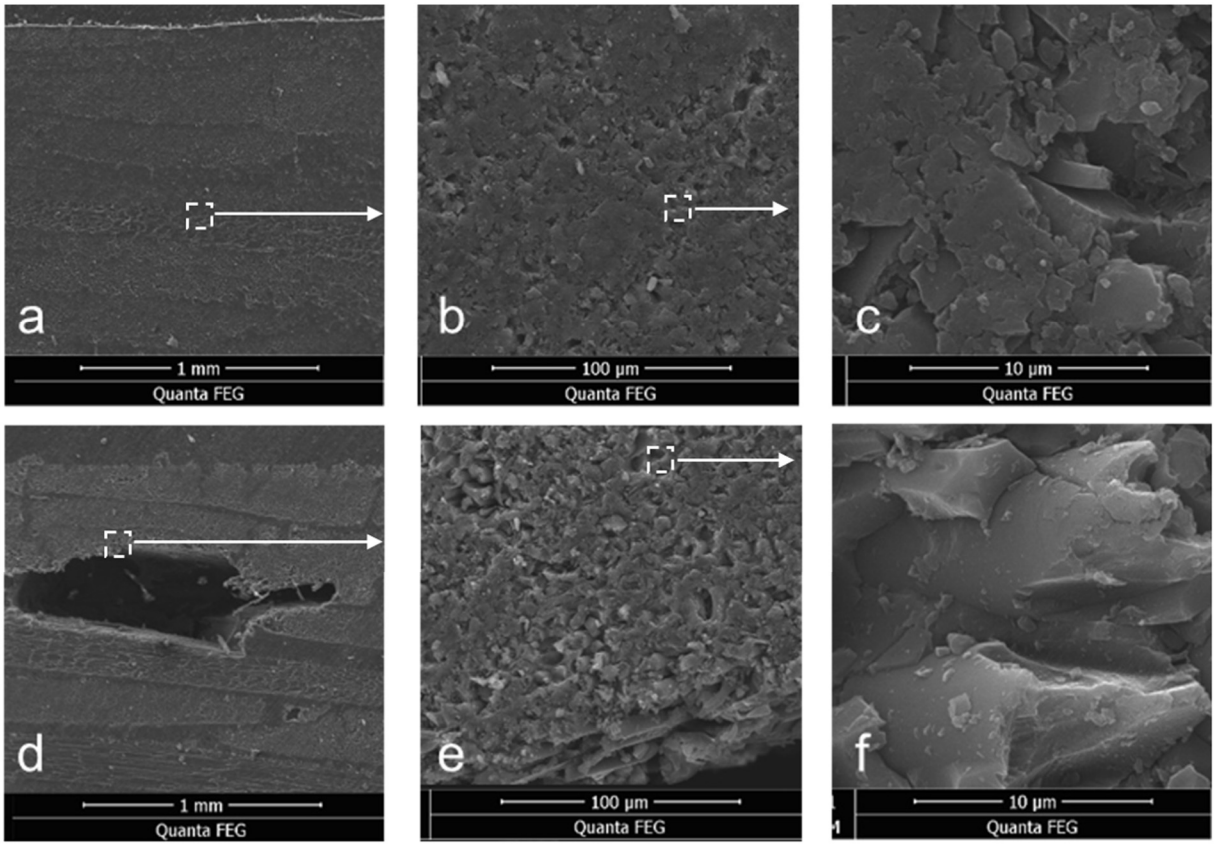

Fig. 17. SEM images of CF/UHTR MC before (a, b, and c) and after the OTB test: AP=90 kJ/cm^2 (d, e, and f).

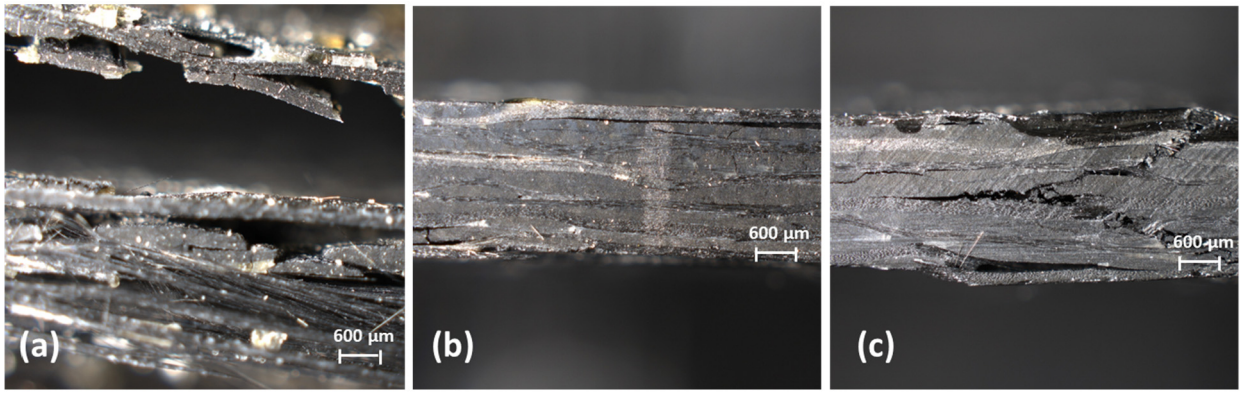

Fig. 18. Microstructure of CF/UHTR laminates after mechanical tests: (a) tensile test; (b) three-point bending; and (c) compressive test.

bon preforms, virgin CF/UHTR and CF/ceramic-UHTR composites, and charred CF/UHTR and CF/ceramic-UHTR composites will be investigated using the synchrotron hard X-ray micro-tomography Beamline 8.3.2 facility at Lawrence Berkeley National Lab/Advanced Light Source (LBL/ALS).

Declaration of competing interest

The authors declare that they have no known competing financial interests or personal relationships that could have appeared to influence the work reported in this paper.

Data availability

Data will be made available on request.

Acknowledgements

This research is partially funded by Techneglas LLC, Perrysburg, OH and KAI, LLC, Austin, TX, USA (KAI-2020-1). The authors acknowledge the use of facilities and the technical assistance of the Advanced Composites International, LLC, Round Rock, TX, USA. The authors acknowledge Hexcel for providing carbon fiber fabrics.

References

[1] J.E. Pavlosky, L.G. St Leger, Apollo experience report: thermal protection subsystem, Apollo Int. Mag. Art Antiq. (1974).
[2] R. Bryan Erb, D.H. Greenshields, L.T. Chauvin, J.E. Pavlosky, C.L. Statham, Apollo thermal-protection system development, J. Spacecr. Rockets 7 (1970) 727–734.
[3] John W. Schaefer, Thomas J. Dahm, David A. Rodriguez, John J. Reese Jr., M.R. Wool, Studies of Ablative Material Performance for Solid Rocket Nozzle Applications, 1967.

[4] B. Laub, E. Laub Venkatapathy, Venkatapathy - 2003 - thermal protection system technology and facility needs for demanding future planetery missions 544 (2004) 239–247.
[5] E.P. Bartlett, L.W. Anderson, D.M. Curry, An evaluation of ablation mechanisms for the apollo heat shield material, J. Spacecr. Rockets 8 (1971) 463–469.
[6] S.D. Williams, D.M. Curry, Thermal protection materials: thermophysical property data 236 (1992).
[7] M. Tauber, et al., Tests of SLA-561V Heat Shield Material for Mars-Pathfinder, Nasa-Tm-110402, 1996.
[8] K.T. Edquist, et al., Mars science laboratory entry capsule aerothermodynamics and thermal protection system, IEEE Aerosp. Conf. Proc. (2007), https://doi.org/10.1109/AERO.2007.352823.
[9] J. Koo, M. Natali, J. Tate, E. Allcorn, Polymer nanocomposites as ablative materials: a comprehensive review, Int. J. Energy Mater. Chem. Prop. 12 (2013) 119–162.
[10] J.H. Koo, L.A. Pilato, Polymer nanocomposite ablatives-part II, Int. J. Energy Mater. Chem. Prop. 19 (2020) 125–187.
[11] J.H. Koo, Polymer Nanocomposites: Processing, Characterization, and Applications, McGraw-Hill Education, 2019.
[12] S. Kim, et al., Development of polyetherimide composites for use as 3D printed thermal protection material, J. Mater. Sci. 55 (2020) 9396–9413.
[13] C.C. Poteet, H. Abu-Khajeel, S.Y. Hsu, Preliminary thermal-mechanical sizing of a metallic thermal protection system, J. Spacecr. Rockets 41 (2004) 173–182.
[14] M.L. Blosser, et al., Development of advanced metallic thermal-protection-system prototype hardware, J. Spacecr. Rockets 41 (2004) 183–194.
[15] J.H. Koo, H. Stretz, J.T. Weispfenning, Z. Luo, W. Wootan, Nanocomposite rocket ablative materials: processing, microstructure, and performance, Collect. Tech. Pap. - AIAA/ASME/ASCE/AHS/ASC Struct. Struct. Dyn. Mater. Conf. 7 (2004) 5090–5104.
[16] M. Natali, M. Monti, D. Puglia, J.M. Kenny, L. Torre, Ablative properties of carbon black and MWNT/phenolic composites: a comparative study, Composites, Part A, Appl. Sci. Manuf. 43 (2012) 174–182.
[17] J.H. Koo, L.A. Pilato, G.E. Wissler, Polymer nanostructured materials for propulsion systems, J. Spacecr. Rockets 44 (2007) 1250–1262.